

WAVELENGTH DEPENDENCE OF THE DIFFERENTIAL  
PATHLENGTH FACTOR AND THE LOG SLOPE IN TIME-RESOLVED  
TISSUE SPECTROSCOPY

M. Essenpreis<sup>1</sup>, M. Cope<sup>2</sup>, C.E. Elwell<sup>1</sup>, S.R. Arridge<sup>2</sup>,  
P. van der Zee<sup>1</sup>, and D.T. Delpy<sup>2</sup>

<sup>1</sup>Department of Medical Physics and Bioengineering  
<sup>2</sup>Department of Computer Science  
University College London  
London, UK

INTRODUCTION

The monitoring of tissue oxygenation by the technique of near infrared spectroscopy (NIRS) was first described by Jobsis in 1977 (Jobsis, 1977). The technique relies upon the relative transparency of tissue to near infrared (NIR) light to enable measurements of changes in optical attenuation across many centimetres of tissue. Early NIRS measurements could only derive qualitative changes in tissue and blood oxygenation from the observed variations in tissue attenuation (Brazy et al., 1985). However, data on the optical pathlength of light in tissue, measured by time resolved techniques employing picosecond laser pulses, have now permitted a quantitative analysis of attenuation measurements to be made (Delpy et al., 1988; Wyatt et al., 1990a). By incorporating information on the optical pathlength into a modified Beer-Lambert law it is possible to quantify changes in chromophore concentration from the measured changes in tissue attenuation. The optical pathlength needed in this calculation, the Differential Pathlength (DP) is defined as the local gradient in a plot of the attenuation measured in a scattering medium versus the absorption coefficient of the medium (Cope et al., 1991a; Cope, 1991b). It has been shown in previous studies (Delpy et al., 1988) that the DP can be approximated by measuring the mean distance that a picosecond light pulse travels across the tissue. Furthermore, a dimensionless multiplying factor, the Differential Pathlength Factor (DPF), can be obtained when the DP is divided by the geometric distance between light source and detector on the tissue surface. This factor has been shown, both theoretically and experimentally, to be approximately constant for any tissue once the optode spacing is larger than about 25 mm (van der Zee et al., 1990; van der Zee et al., in press), enabling clinical NIRS measurements to be made with varying optode geometries. Two instruments are now commercially available which make use of this property of the DPF to calculate

width of a single pulse from the laser was about 2 ps (full width half maximum) and the repetition rate was 82 MHz.

To allow flexible application of the light to the tissue, the laser output was coupled into a single low dispersion fibre (Corning SDF, 125  $\mu\text{m}$  diameter, 0.6 m length). Part of the laser output was used both as a time reference and as a trigger for the detector, a synchroscan streak camera (C1587, Hamamatsu Photonics Ltd). The streak camera was operated at its slowest sweep speed in order to sample a large part of the TPSF in one streak image. In this mode, the temporal calibration of the camera was  $\tau = 4.95$  ps per channel and the streak width 2.53 ns. The overall temporal resolution of the system was about 10 ps. A one metre long fibre bundle with a circular cross section (1.9 mm diameter) was used to collect light emerging from the tissue. At the camera end, the fibres were aligned in a linear array across the streak camera input slit. The individual fibres in the bundle (Corning SDF) were all the same length ( $\pm 1$  mm) to minimise transit time distribution. Incorporated into the row of fibres was a single additional fibre into which the time reference light pulse was coupled. Since the light pulse passing through this reference fibre was acquired on the same streak image together with the light from the sample, it could be used to accurately time the photons emerging from the tissue and to correct for the colour delay of the streak camera.

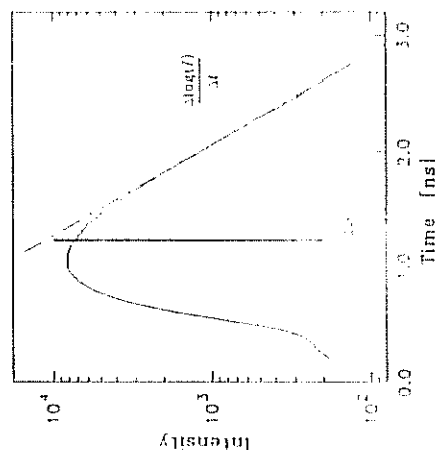


FIGURE 2. A typical Temporal Point Spread Function showing the mean time  $\langle t \rangle$  and the logarithmic slope of the intensity decay (measured on the head of an adult).

### Characterization of Temporal Point Spread Functions

Light is multiply scattered in tissue, so the photons injected in a picosecond laser pulse take different paths of varying length in travelling from the source to the detector fibre. Thus, photons which travel over a different total distance will arrive at different times at the detecting fibre bundle. This gives rise to an intensity distribution with time which is spread out broadly and shifted in time with respect to the picosecond input pulse. An example of such an intensity distribution is shown in Figure 2. The data shown was collected at 760 nm on the head of an adult using an optode spacing of

variations in the concentrations of haemoglobin and cytochrome aa<sub>3</sub> from spectral changes measured at the bedside (NIRO 1000 and NIRO 500, Hamamatsu Photonics KK, Japan). Using these instruments, methods for absolute quantitation of cerebral blood flow and blood volume have been developed, and measurement of these parameters made in newborn infants (Edwards et al., 1988; Wyatt et al., 1990b) and adult humans (Elwell et al., in press).

It is known from theoretical and experimental studies that both the absorption and the scattering coefficient effect the Temporal Point Spread Function (TPSF) of an object, the latter being defined as the temporal response of the light intensity exiting the object following an input impulse function (Delpy et al., 1988). Time resolved measurements on tissue at a single wavelength have demonstrated these effects, the DPF for individual tissues being different (van der Zee et al., in press), and varying slightly with changes in attenuation (Delpy et al., 1989). It is the purpose of this paper to investigate the wavelength dependence of the TPSF of various tissues since the addition of this information into the modified Beer Lambert law would further improve the accuracy of the calculated chromophore concentrations. The TPSF is a complex function of both the fundamental optical properties of the tissue and of the measurement geometry, but in this study, the variation with wavelength of two parameters characterizing the TPSF are analyzed: The Differential Pathlength Factor and the logarithmic slope of the intensity decay with time ( $K_D$ ). Experimental measurements of these parameters have been made over a wavelength range between 740 nm and 840 nm, on the normoxic adult head, calf and forearm, and across the head of a rat at varying levels of blood oxygenation and blood content.

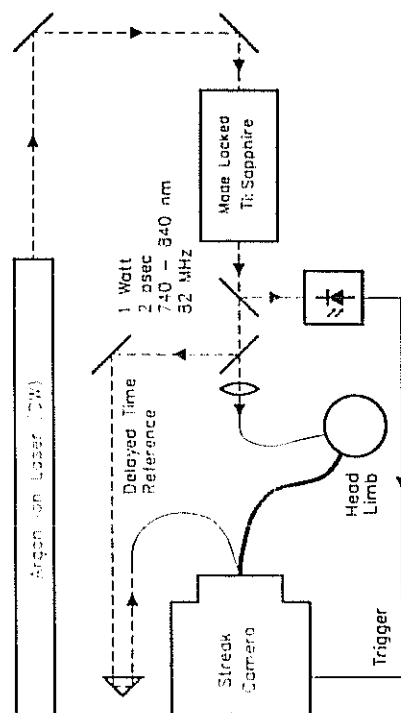


FIGURE 1. Experimental system for the measurement of the wavelength dependence of the TPSF in tissue.

### EXPERIMENTAL TECHNIQUE

The experimental system used to measure the TPSF is shown in Figure 1. The light source was a mode-locked Ti:Sapphire laser (Tsunami, Spectra Physics Ltd) pumped by a 12 W Argon ion laser (Model 2040, Spectra Physics Ltd). The mirror set of the Ti:Sapphire laser allowed for tunability between 740 nm and 840 nm. The pulse

40 mm. Indicated on this figure are the mean time  $\langle t \rangle$  of the intensity distribution and  $\log(I)/t$ , the gradient of the linear part of the intensity decay following the initial intensity maximum.  $\langle t \rangle$  was calculated by integrating over the TPSF:

$$\langle t \rangle = \frac{\int_0^{\infty} t I(t) dt}{\int_0^{\infty} I(t) dt} \quad (1)$$

where  $I(t)$  is the intensity of the light recorded by the streak camera as a function of time  $t$ .  $K_B$  was calculated using linear regression within a window defined by percentages of the intensity maximum. Regression started at 10% and ended at 2% of the maximum intensity for each TPSF.  $K_B$  (in units of length<sup>-1</sup>) can then be expressed as:

$$K_B = - \frac{\Delta \log(I(t))}{\Delta t} = - \frac{n_1}{c} \cdot \frac{\Delta \log(I(t))}{\Delta t} \quad (2)$$

with  $\Delta l = \Delta t \times c/n_1$ ,  $c$  being the speed of light in vacuum and  $n_1$  the refractive index of the tissue. For all the data described here, a value for  $n_1$  of 1.40 was assumed (Bolin et al., 1989). The DPF is calculated from the measured TPSF by multiplying the mean time with the speed of light in tissue and dividing by the physical length (chord length)  $d$  between source and detector fibres:

$$DPF = \frac{DP}{d} = \frac{1}{d} \cdot \frac{c}{n_1} \langle t \rangle \quad (3)$$

#### Experimental Procedure for Studies on Adult Humans

As in studies reported previously (van der Zee et al., in press), the TPSF has been measured on the head, forearm and calf of a group of male and female adult volunteers. The age of the subjects was between 17 and 55 years (median 26 years), and they had no known muscular or circulatory disorders. Measurements were made on the limbs of 6 subjects and on the head of 7 subjects. A wavelength scan consisted of thirteen separate measurements between 740 nm and 840 nm at intervals of approximately 5 nm between 750 nm and 770 nm, and 10 to 15 nm below 750 nm and above 770 nm. More frequent sampling was applied around 760 nm to accurately measure the more rapid spectral change of the TPSF predicted to occur around the 760 nm absorption peak of deoxy-haemoglobin (Wray et al., 1988). A full set of measurements on one subject was typically completed within 30 minutes.

For measurements on the leg or arm, the subjects were seated comfortably and the limb was placed in a U-shaped rest into which holes were drilled which enabled both the transmitting and receiving fibres to be placed in contact with the skin from below. The fibres were either positioned over the muscles on the medial aspect of the forearm away from any palpable bone, or on the rear surface of the calf muscle at the broadest part of the leg. The optode spacing was approximately 40 mm for all the studies. Care was taken that the blood supply to the tissues was not obstructed whilst the limb lay in the apparatus by supporting the wrist or heel on an adjustable rest. Interference from background light was reduced by wrapping the limb with a black cloth.

The procedure for measurements made on the head was similar to that reported in previous studies (van der Zee et al., in press). The receiving fibre bundle was positioned over the temple, with the transmitting fibre on the upper forehead approximately 40 mm away. Figure 3 shows the TPSF at several wavelengths measured on the head of one subject. The change in both the position and the shape of the TPSF with wavelength can be clearly seen.

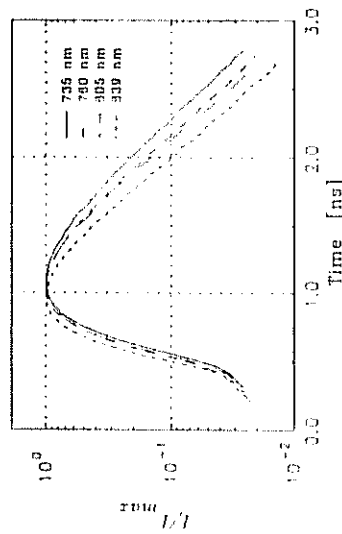


FIGURE 3. TPSFs measured at selected wavelengths (735 nm, 760 nm, 805 nm and 839 nm) on the head of one subject.

#### Experimental Procedure and Preparation for Study on Adult Rat Brain

TPSF measurements were also made on the brain of an adult Wistar rat. Following anaesthesia (Urethane 36% w/v intraperitoneal, 5 ml kg<sup>-1</sup>), the temporoparietal muscles were reflected, the skull exposed and cleared of residual surface tissue. A tracheal cannula was inserted to allow easy ventilation and manipulation of inspired gas concentrations, and a femoral artery was cannulated for blood sampling. The head of the animal was immobilised in a stereotaxic frame. The transmitting fibre and the receiving fibre bundle were fixed in diametrically opposed positions across the head, the ends of the fibres being in contact with the skull via an optical coupling gel (Math Associates Inc, Westbury, NY, USA). Measurements of the TPSF were made with the animal breathing 47% and 30% oxygen (balance N<sub>2</sub>). Finally, with the animal breathing 100% oxygen, an exchange transfusion with saline was performed until the animal died (residual haematocrit < 5%). A TPSF scan was then performed immediately post mortem. The rat head diameter (and hence optode spacing) was measured at the end of the study.

#### RESULTS

The DPF and  $K_B$  were calculated for each set of TPSFs and then linearly interpolated to 5 nm intervals. For each tissue studied, the values for the DPF and  $K_B$  at each wavelength were then averaged over all the subjects, and the corresponding standard deviations (SD) were calculated. Figure 4 summarises these results, showing the DPF and  $K_B$  as a function of wavelength for the head (Figure 4(a)), the forearm (Figure 4(b)), the male calf (Figure 4(c)) and the female calf (Figure 4(d)).

FIGURE 4 c/d. Changes with wavelength of the DPF and  $K_{ls}$  in the adult male calf (c) and the adult female calf (d). Data are the average for all subjects  $\pm$  one standard deviation.

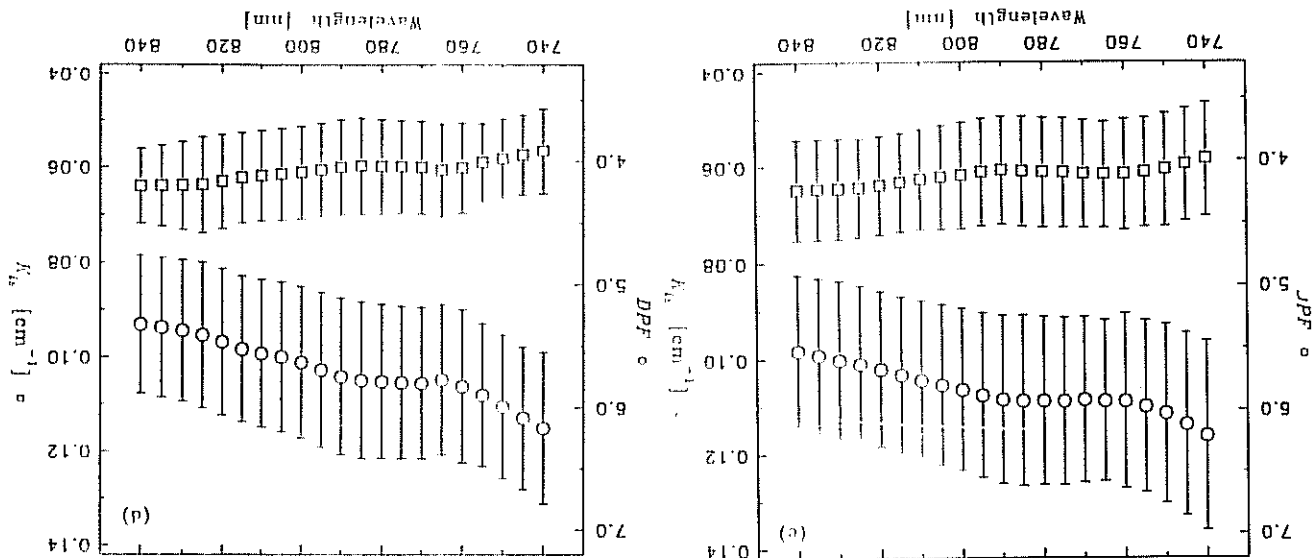
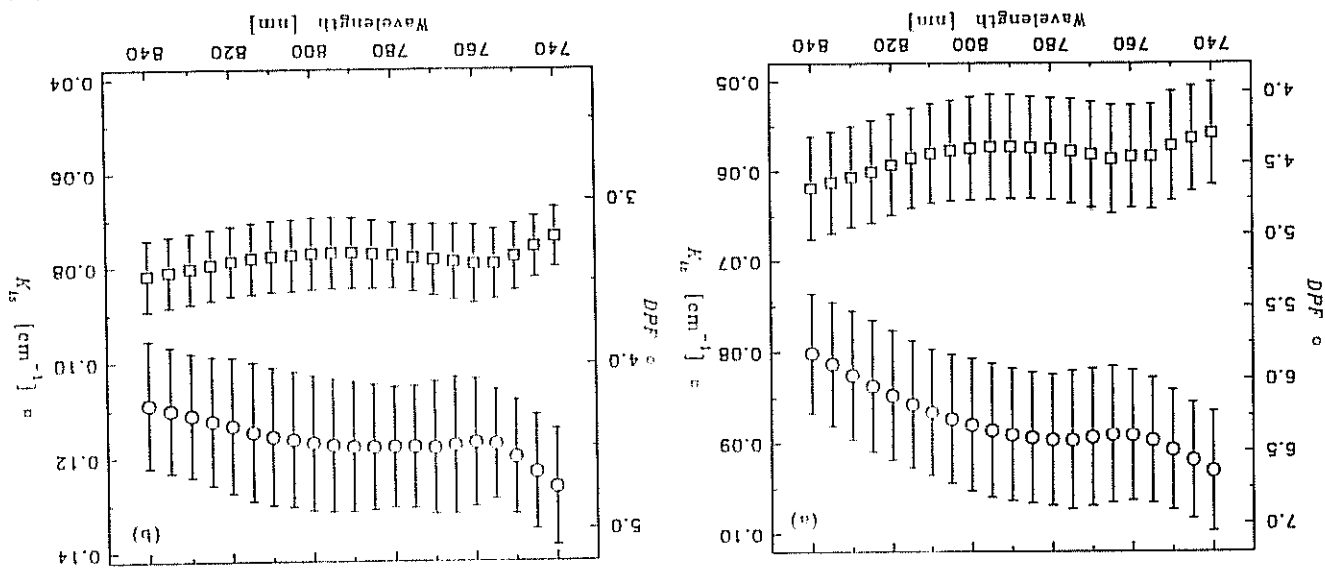


FIGURE 4 a/b. Changes with wavelength of the DPF and  $K_{ls}$  in the adult head (a) and the adult forearm (b). Data are the average for all subjects  $\pm$  one standard deviation.



The data for the DPF measured on the rat brain are shown in Figure 5(a) and the corresponding data for  $K_{1s}$  in Figure 5(b). For the sake of clarity, error bars for the inherent SD of the measurement of the DPF have been omitted. In a previous study (van der Zee et al., in press) these have been shown by repeated measurement at one site to be less than 5%.

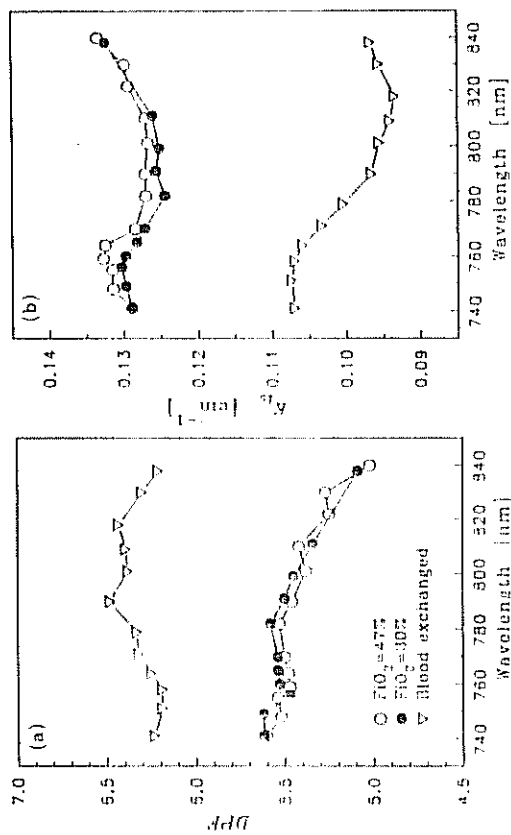


FIGURE 5. Changes with wavelength of the DPF (a) and  $K_{1s}$  (b) in the brain of an adult rat at two levels of FIO<sub>2</sub> and following saline exchange transfusion.

## DISCUSSION

A number of features common to the DPF and  $K_{1s}$  spectra of all the tissues studied can be observed.

Firstly, a local minimum in the DPF can be seen around 760 nm. This coincides with a known peak in the absorption spectrum of deoxyhaemoglobin (Hb). Since all of the studies on humans were made under normoxic conditions, the amount of Hb would be expected to be small, and this is reflected in the magnitude of the observed peak. The general reduction of the DPF due to the increased tissue absorption is in agreement with experimental and theoretical predictions (Delpy et al., 1989; Cope et al., 1991a). The general fall in the DPF beyond 800 nm can be partly explained by the same argument, since the absorption of oxyhaemoglobin (HbO<sub>2</sub>) increases beyond 800 nm. However, the DPF spectrum also shows a decline over the whole of the 740 - 840 nm range. This is a consequence of the effects of tissue scattering. Light scattering by tissue is very anisotropic in its angular distribution (van der Zee and Delpy, 1988), a feature which is a characteristic of large particle or Mie scattering. The wavelength dependence of Mie scattering results in a fall in both the reduced scattering coefficient

(van der Zee et al., 1991) and the scattering efficiency (Bohren and Huifman, 1983), and both of these would result in a reduction of DPF with wavelength (Cope et al., 1991a). The data for DPF in each of the human tissues are consistent with these explanations, the DPF measured in the arm and calf (where myoglobin is present as an additional absorber of light) being smaller than those for the head.

Secondly, the  $K_{1s}$  spectra are approximately mirror images of their corresponding DPF spectrum. The value of  $K_{1s}$  has previously been interpreted as representing the absorption coefficient of the tissues (Chance et al., 1988a; Chance et al., 1988b), although this is in fact only true in extremely limited circumstances (Jacques and Flock, 1991; Patterson et al., 1990). In these results, the  $K_{1s}$  values for calf and forearm are higher than those for the head, although the differences are smaller than expected. In addition, the absolute magnitudes are not in agreement with published data for the absorption coefficient of muscle (Cheong et al., 1990) and brain (Sierrenborg et al., 1990). The reasons for this discrepancy are still the subject of study, although it is thought most likely to be due to the effects of measurement geometry and finite boundaries (Madsen et al., 1991).

Thirdly, both the DPF and  $K_{1s}$  data in Figure 4 exhibit a large standard deviation. This is not due to error in the measurement technique, which has been shown previously to be smaller than 5%, but instead represents a true inter-subject variation. The absolute magnitudes of the mean DPF obtained in this study are also different from those reported previously, but measured on a different group of volunteers (van der Zee et al., in press). The most striking difference between these two studies are in the data from the adult calf. In the previous study, a significant difference in DPF was observed between male and female subjects, and this was attributed to male female differences in fat/muscle ratio. In this study, the difference although present, is not significant. One can speculate that since the major difference appears to be in the DPF of the male calf (at a wavelength of 760 nm the DPF is 5.93 in this study compared to 3.98 in the previous study), the subjects employed in this present study were significantly less fit! The overall inter-subject variability probably arises from variation both in the anatomy of the tissues (Maughan et al., 1984), and in its physiological status, especially the tissue blood volume and oxygenation (Sakai et al., 1985). These variations set a limit to the accuracy with which spectroscopic data can presently be quantitated. Recent developments of techniques for measuring optical pathlength at the bedside should overcome this limitation (Lakowicz and Bernini, 1990; Sevick and Chance, 1991).

The general features of the DPF and  $K_{1s}$  spectra measured on the rat brain (Figure 5) are similar to those of the human head. A small, but still observable local minimum in DPF occurs around 760 nm, and DPF decreases with wavelength beyond 800 nm. Again, the  $K_{1s}$  spectrum appears to be approximately a mirror image of the DPF spectrum. There was no significant change in both spectra as the FIO<sub>2</sub> was lowered from 47% to 30%, but this is only to be expected, since PaO<sub>2</sub> only dropped from 12.4 to 12.1 kPa, a value which would still result in an arterial haemoglobin saturation of 97%. A change in the tissue absorption coefficient is therefore not expected and the very similar DPF and  $K_{1s}$  spectra (Figure 5) reflect this. Note however that the magnitude of  $K_{1s}$  is far higher than that measured on the human brain. This marked overestimate is a consequence of the effects of the much closer tissue boundary in the small rat head. The effects of the exchange transfusion are dramatic, the DPF increasing by approximately 16% and  $K_{1s}$  falling by 21%. This change, due to an overall decrease in tissue attenuation is similar to that reported previously (Delpy et al., 1989), and again illustrates a possible source of error in the calculation of NIRS data.

## CONCLUSIONS

We have shown experimentally the spectral dependence of the Differential Pathlength Factor and the log slope in the NIR. In general, the experimental results are in agreement with theoretical predictions. The DPF increases with wavelength and shows a local minimum at 760 nm, coinciding with the absorption peak of Hb.  $K_{is}$  was found to show inverse behaviour to the DPF spectrum, increasing with wavelength and revealing a local maximum at 760 nm. However, the absolute magnitude of  $K_{is}$  was not equal to the absorption coefficient of the tissues known from previous studies.

The importance of the DPF in quantitating NIRS data has previously been established. The inter subject variation in the absolute magnitude of the DPF shown in this and in previous studies sets a limit on the accuracy with which chromophore concentrations can be calculated. This variation in the DPF is typically about  $\pm 10\%$ , and its source of error could only be eliminated if the DPF were measured on each patient. In addition, the spectral variation in DPF shown in this study demonstrates that further improvements in the accuracy of chromophore estimation can be obtained if a wavelength dependent DPF is used in the modified Beer Lambert law. The most accurate estimation of tissue chromophore concentration will only come from NIRS systems that not only measure changes in attenuation at several wavelengths, but also continuously monitor optical pathlength at each wavelength.

**ACKNOWLEDGEMENTS**-The work described in this paper was supported by grants from the Wellcome Trust, SERC, MRC, the Wolfson Foundation and Hamamatsu Photonics KK. We also thank Spectra Physics UK for the loan of the Tsunami laser system. M. Essenpreis is grateful for the financial support of the Gottlieb Daimler- und Karl Benz-Stiftung.

## REFERENCES

- Bohren C.F. and Huifman D.R. (1983) Absorption and Scattering of Light by Small Particles, J. Wiley (New York).
- Bolin F.P., Preuss L.E., Taylor R.C., Ference R. (1989) Refractive index of some mammalian tissues using a fibre optic cladding method. Applied Optics, 28:2297-2302.
- Brazy J.E., Lewis D.V., Mirmick M.H., Jöbsis F.F. (1985) Noninvasive monitoring of cerebral oxygenation in preterm infants: preliminary observations. Pediatrics, 75:217-225.
- Chance B., Leigh J.S., Miyake H., Smith D.S., Nioka S., Greenfield R., Finander M., Kaufmann K., Levy W., Young M., Cohn P., Yoshioka H., Boretzky R. (1988a) Comparison of time resolved and unresolved measurements of deoxyhaemoglobin in brain. Proc. Nat. Acad. Sci., 85:4971-4975.
- Chance B., Nioka S., Kent J., McCully K., Fountain M., Greenfield R., Holtom G. (1988b) Time resolved spectroscopy of haemoglobin and myoglobin in resting and ischaemic muscle. Anal. Biochem., 174:698-707.
- Cheong W.-F., Praeli S.C., Welch A.J. (1990) A review of the optical properties of biological tissues. IEEE J. Quant. Electron., 26:2166-2185.
- Cope M., van der Zee P., Essenpreis M., Arridge S.R., Delpy D.T. (1991a) Data analysis methods for near infrared spectroscopy of tissue: problems in determining the relative cytochrome  $aa_3$  concentration. Proc. SPIE, 1431:251-262.

- Cope M. (1991b) The development of a near infrared spectroscopy system and its application for non invasive monitoring of cerebral blood and tissue oxygenation in the newborn infant. PhD Thesis, University of London.
- Delpy D.T., Cope M., van der Zee P., Arridge S.R., Wray S., Wyatt J.S. (1988) Estimation of optical pathlength through tissue from direct time of flight measurement. Phys. Med. & Biol., 33:1433-1442.
- Delpy D.T., Arridge S.R., Cope M., Edwards A.D., Reynolds E.O.R., Richardson C.E., Wray S., Wyatt J.S., van der Zee P. (1989) Quantitation of pathlength in optical spectroscopy. Adv. Exp. Med. & Biol., 248:41-46.
- Edwards A.D., Wyatt J.S., Richardson C.E., Delpy D.T., Cope M., Reynolds E.O.R. (1988) Cerebral blood flow in ill newborn infants by near infrared spectroscopy. Lancet ii, 770-771.
- Elwell C.E., Cope M., Edwards A.D., Wyatt J.S., Reynolds E.O.R., Delpy D.T. (in press) Measurement of cerebral blood flow in adult humans using near infrared spectroscopy - methodology and possible errors. Adv. Exp. Med. & Biol.
- Jacques S.L. and Floek S.T. (1991) Effect of surface boundary on time resolved reflectance: measurement with a prototype endoscopic catheter. Proc. SPIE, 1431:12-20.
- Jöbsis F.F. (1977) Non invasive, infrared monitoring of cerebral and myocardial oxygen sufficiency and circulatory parameters. Science, 198:1264-1267.
- Lakowicz J.R. and Berndt K. (1990) Frequency domain measurements of photon migration in tissues. Chem. Phys. Lett., 166:246-252.
- Madsen S.J., Patterson M.S., Wilson B.C., Park Y.D., Moulton J.D., Jacques S.L., Hefetz Y. (1991) Time resolved diffuse reflectance and transmittance studies in tissue simulating phantoms: a comparison between theory and experiment. Proc. SPIE, 1431:42-51.
- Maughan R.J., Watson J.S., Weir J. (1984) The relative proportions of fat, muscle and bone in the normal human forearm as determined by computer assisted tomography. Clin. Sci., 66:683-689.
- Patterson M.S., Moulton J.D., Wilson B.C., Chance B. (1990) Applications of time resolved light scattering measurements to photodynamic therapy dosimetry. Proc. SPIE, 1203:62-75.
- Sakai F., Nakazawa K., Tazaki Y., Ishii K., Hidetada H., Igarashi H., Nanda T. (1985) Regional cerebral blood volume and haematocrit measured in normal human volunteers by single-photon emission computed tomography. J. Cereb. Blood Flow and Metabolism, 5:207-213.
- Sevick E.M. and Chance B. (1991) Photon migration in a model of the head measured using time and frequency domain techniques: potentials of spectroscopy and imaging. Proc. SPIE, 1431:84-96.
- Sternberg H.J.C.M., van Gemert M.J.C., Kamphorst W., Wolbers J.G., Hogervorst W. (1989) The spectral dependence of the optical properties of human brain. Lasers in Med. Sci., 4:221-227.
- Wray S., Cope M., Delpy D.T., Wyatt J.S., Reynolds E.O.R. (1988) Characterisation of the near infrared absorption spectra of cytochrome  $aa_3$  and haemoglobin for the non invasive monitoring of cerebral oxygenation. Biochim. Biophys. Acta., 933:184-192.
- Wyatt J.S., Cope M., Delpy D.T., van der Zee P., Arridge S.R., Edwards A.D., Reynolds E.O.R. (1990a) Measurement of optical pathlength for cerebral near infrared spectroscopy in newborn infants. Dev. Neuroscience, 12:140-144.
- Wyatt J.S., Cope M., Delpy D.T., Richardson C.E., Edwards A.D., Wray S.C., Reynolds E.O.R. (1990b) Quantitation of cerebral blood volume in newborn infants by near infrared spectroscopy. J. Appl. Physiol., 68(3):1086-1091.

- van der Zee P. and Delpy D.T. (1988) Computed point spread functions for light in tissue using a measured volume scattering function. *Adv. Exp. Med. & Biol.* 222:191-197.
- van der Zee P., Arridge S.R., Cope M., Delpy D.T. (1990) The effect of optode positioning on optical pathlength in near infrared spectroscopy of brain. *Adv. Exp. Med. & Biol.* 277:79-84.
- van der Zee P., Essenpreis M., Delpy D.T., Cope M. (1991) Accurate determination of the optical properties of biological tissues using a Monte Carlo inversion technique. *Proc. ICO Meeting on Atmospheric, Volume and Surface Scattering and Propagation*, Florence, Italy, August 27-30, 1991.
- van der Zee P., Cope M., Arridge S.R., Essenpreis M., Potter L.A., Edwards A.D., Wyatt J.S., McCormick D.C., Roth S.C., Reynolds E.O.R., Delpy D.T. (in press) Experimentally measured optical pathlengths for the adult head, cat and forearm and the head of the newborn infant as a function of interoptode spacing. *Adv. Exp. Med. & Biol.*

## TOWARDS HUMAN BRAIN NEAR INFRARED IMAGING: TIME RESOLVED AND UNRESOLVED SPECTROSCOPY DURING HYPOXIC HYPOXIA

M. Ferrari<sup>1</sup>, R.A. De Blas<sup>2</sup>, F. Safou<sup>2</sup>, Q. Wei<sup>2</sup>, and G. Zaccanti<sup>1</sup>

<sup>1</sup>Dipartimento di Scienze e Tecnologie Biomediche, Università dell'Aquila, Italy and Laboratorio di Biologia Cellulare, Istituto Superiore di Sanità, Istituto di Anestesiologia e Rianimazione, I Università di Roma, Roma, Italy; <sup>2</sup>Dipartimento di Fisica, Università di Firenze, Firenze, Italy

### INTRODUCTION

Near infrared (IR) spectroscopy (NIRS) on animals and humans originated from the work of Jobsis (1977). Early cerebral and muscle NIRS measurements using multi-wavelength photometers were only qualitative. Fast scanning spectrophotometry has been utilized for a better spectral analysis and quantification purposes (Ferrari et al., 1989). Only pulse time and phase modulation spectroscopies can calculate pathlength in brain and muscle. Optical imaging in the near IR using these time-resolved methods is currently pursued by different groups (Chance, 1991 for a review). There are however significant technical and clinical problems related to the imaging technique yet to be solved before it can become truly a routine clinical tool.

When transmitting picosecond laser pulses and detecting photons on the opposite side of the object, the contrast can be strongly enhanced by detecting only the photons with the shortest traveling time. Short time resolution would restrict the scattering path and could provide further amelioration in image definition. Recently, Hitachi research laboratories (Shinohara et al., 1991, and this volume) obtained images of rat brain oxygenation during middle cerebral artery ischemia using dual wavelength picosecond near IR laser technique combined with conventional back projection image reconstruction. The aim of this paper was to investigate human brain oxygenation changes during hypoxic hypoxia using two wavelength picosecond near IR laser spectroscopy. Pathlengths were mapped on the human forehead. By combining spectral information obtained by a fast scanning spectrometer with pathlength data it was possible to quantify oxy- and deoxy-hemoglobin (Hb) concentration changes during hypoxic hypoxia.

FIGURE CAPTIONS

Figure 1: Experimental system for the measurement of the wavelength dependence of the TPSF in tissue.

Figure 2: A typical Temporal Point Spread Function showing the mean time  $\langle t \rangle$  and the logarithmic slope of the intensity decay (measured on the head of an adult).

Figure 3: TPSFs measured at selected wavelengths (735 nm, 760 nm, 805 nm and 839 nm) on the head of one subject.

Figure 4: Changes with wavelength of the DPF and  $K_t$  in the adult head (a), the adult forearm (b), the adult male calf (c), and the adult female calf (d). Data are the average for all subjects  $\pm$  one standard deviation.

Figure 5: Changes with wavelength of the DPF (a) and  $K_t$  (b) in the brain of an adult rat at two levels of  $\text{FiO}_2$ , and following saline exchange transfusion.

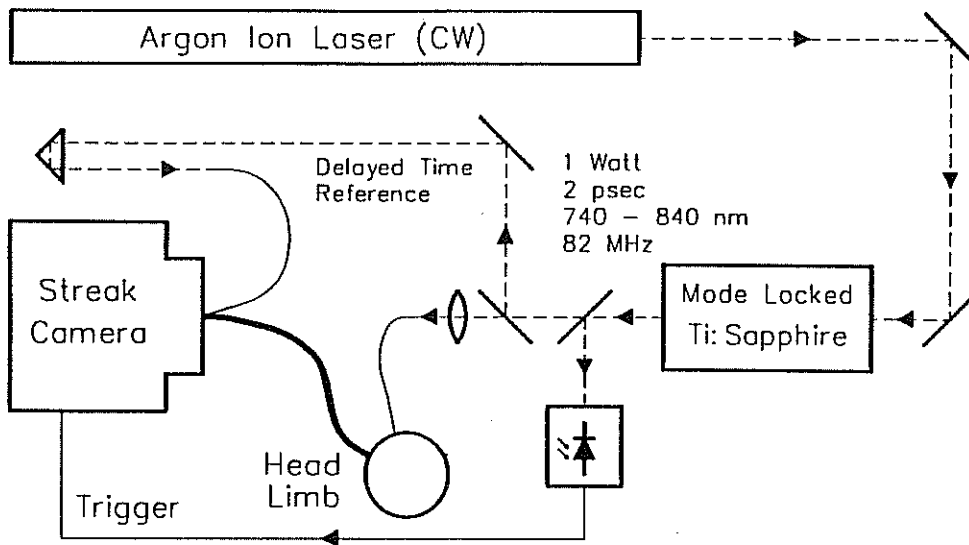


Figure 1: Experimental system for the measurement of the wavelength dependence of the TPSF in tissue.

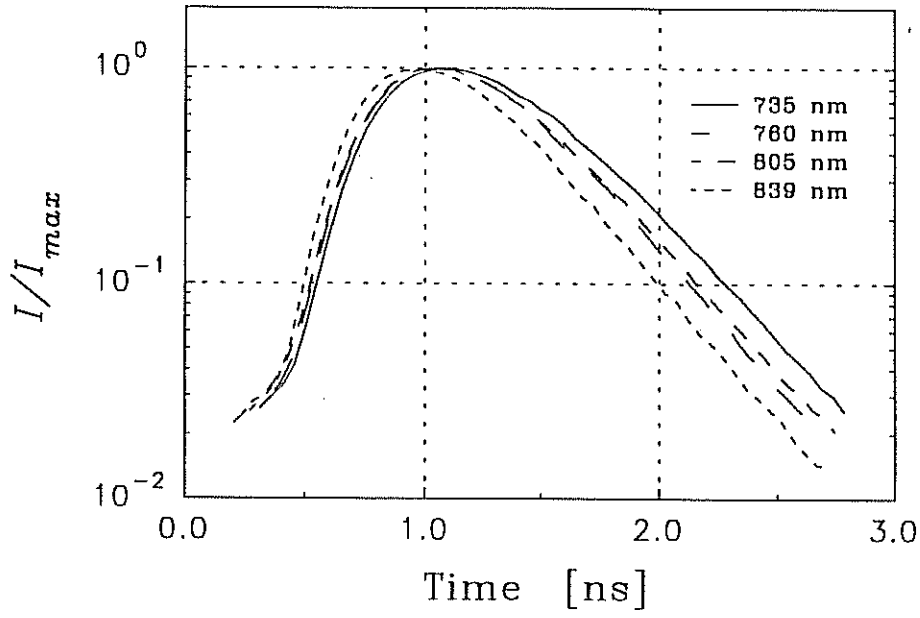


Figure 3: TPSFs measured at selected wavelengths (735 nm, 760 nm, 805 nm and 839 nm) on the head of one subject.

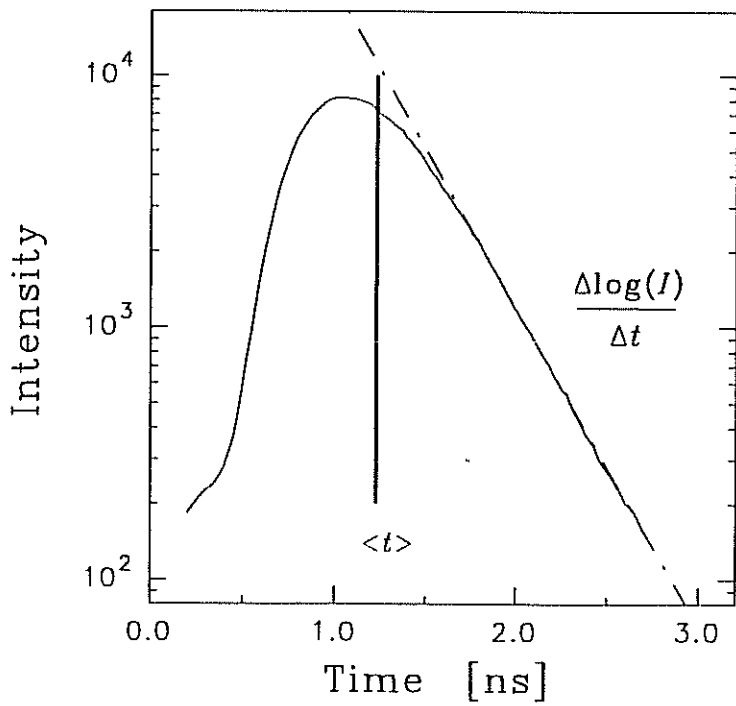


Figure 2: A typical Temporal Point Spread Function showing the mean time  $\langle t \rangle$  and the logarithmic slope of the intensity decay (measured on the head of an adult).

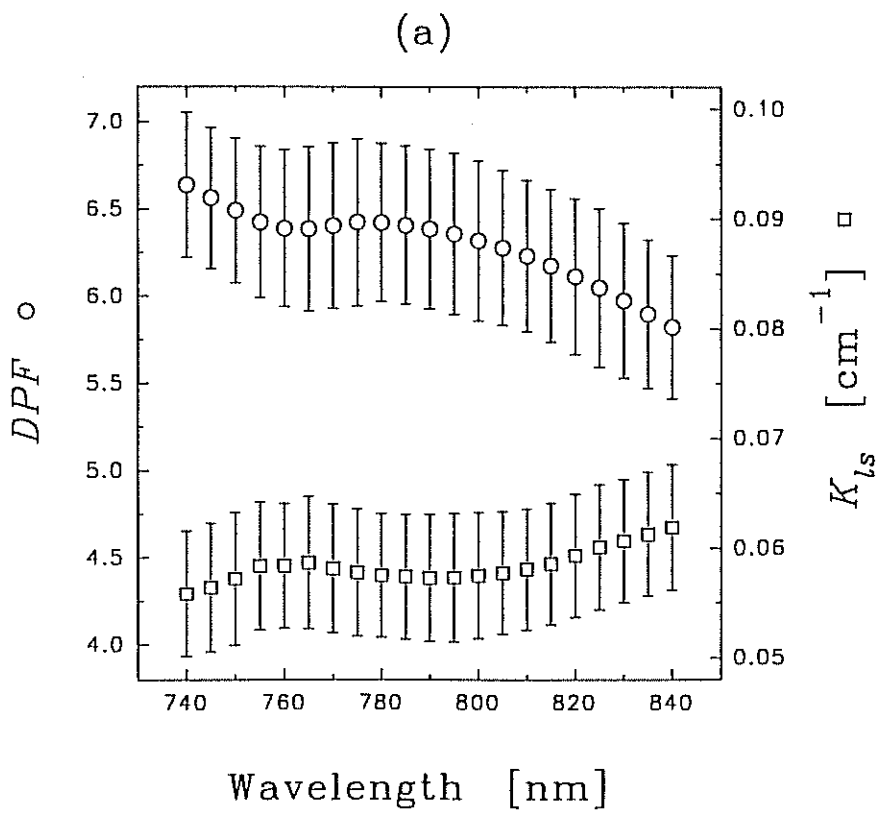
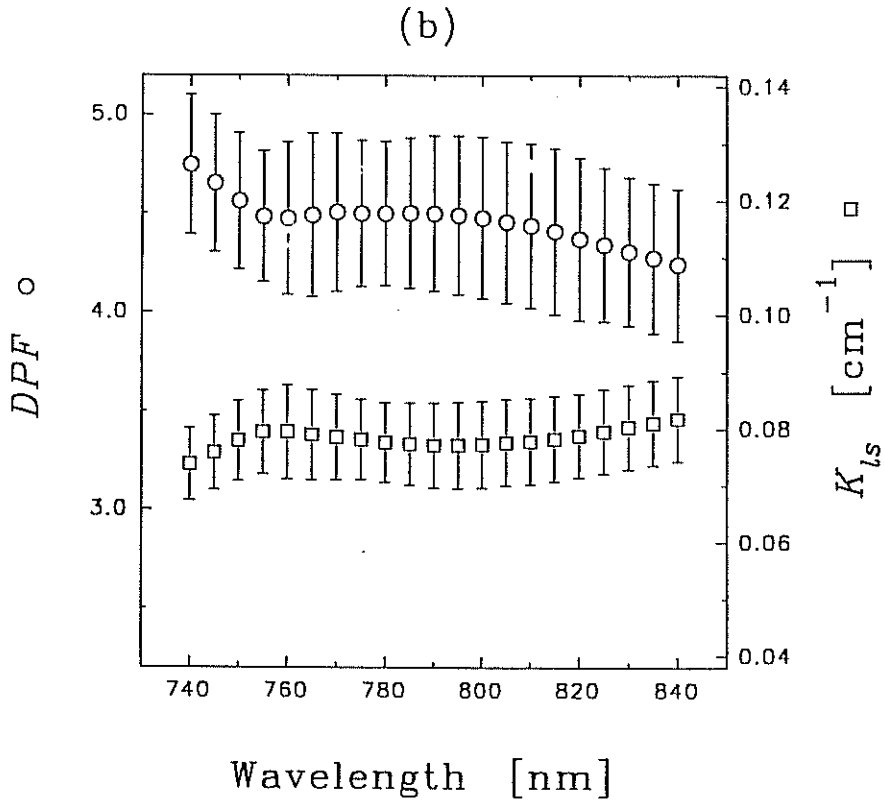
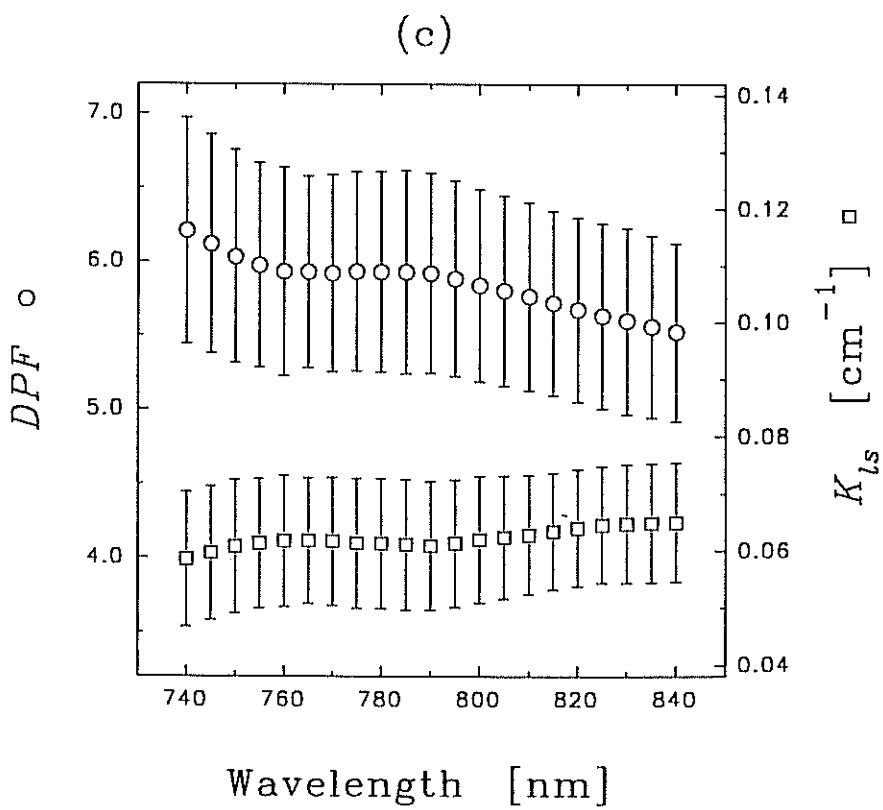
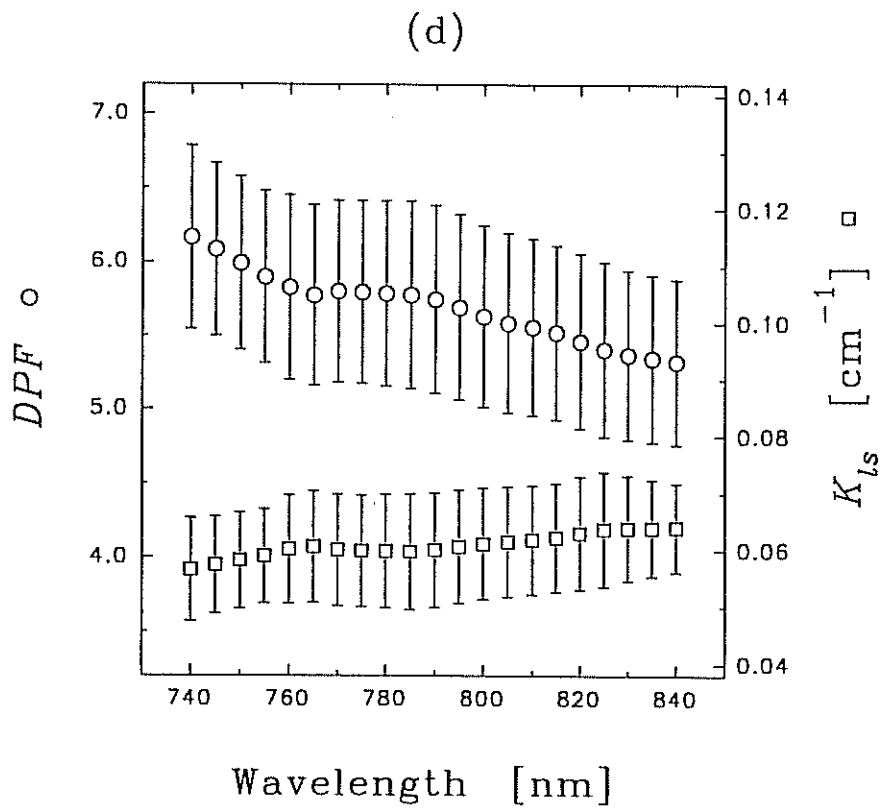


Figure 4: Changes with wavelength of the DPF and  $K_{ls}$  in the adult head (a), the adult forearm (b), the adult male calf (c), and the adult female calf (d). Data are the average for all subjects  $\pm$  one standard deviation.

Figure 4



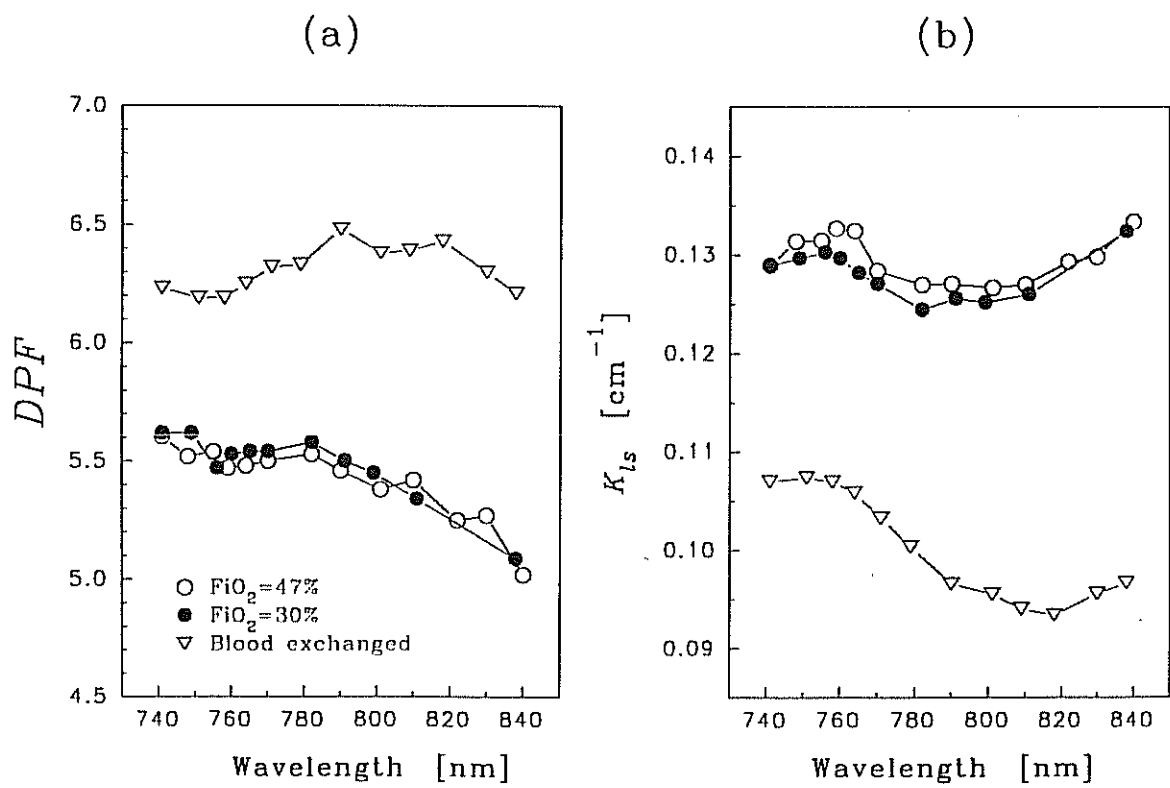


Figure 5: Changes with wavelength of the DPF (a) and  $K_{ls}$  (b) in the brain of an adult rat at two levels of  $FiO_2$ , and following saline exchange transfusion.